

# **A 12 Building model Hamiltonians for strongly correlated materials**

E. Pavarini

Institut für Festkörperforschung

Forschungszentrum Jülich GmbH

## **Contents**

<b>1</b>	<b>Introduction</b>	<b>2</b>
<b>2</b>	<b>From ab-initio to many-body model Hamiltonians</b>	<b>2</b>
<b>3</b>	<b>Realistic many-body models from LDA</b>	<b>5</b>
3.1	From the Bloch to the Wannier representation . . . . .	5
3.2	Electronic structure calculations with the NMTO method . . . . .	6
3.3	Downfolding and NMTO Wannier functions . . . . .	9
3.4	Wannier functions as a basis for the Hubbard model . . . . .	12
<b>4</b>	<b>DMFT solution of realistic many-body models</b>	<b>14</b>
4.1	Dynamical mean-field theory . . . . .	14
4.2	LDA+DMFT . . . . .	16
<b>5</b>	<b>Application to orthorhombic 3d<sup>1</sup> perovskites</b>	<b>17</b>
<b>6</b>	<b>Concluding remarks</b>	<b>19</b>
<b>A</b>	<b>Atomic units</b>	<b>20</b>

# 1 Introduction

In the last decades, the discovery of high-temperature superconductivity in cuprate oxides (e.g.  $\text{YBa}_2\text{Cu}_3\text{O}_7$ ) and of colossal magneto resistance in manganites (e.g.  $\text{La}_{1-x}\text{Sr}_x\text{MnO}_3$ ) have driven a lot of attention toward transition metal oxides [1]. The properties of these systems are very sensitive to doping, pressure and temperature; transition metal oxides could therefore become the building blocks for future technologies. The varieties of exotic phenomena that these materials exhibit — from unconventional superconductivity and striped phases (e.g.  $\text{La}_{1-x}\text{Sr}_x\text{CuO}_4$ ) to Mott insulating behavior (e.g.  $\text{V}_2\text{O}_3$ ), charge (e.g.  $\text{La}_{0.5}\text{Ca}_{0.5}\text{MnO}_3$ ) and orbital (e.g.  $\text{LaMnO}_3$ ) ordering — are believed to be the effects of the interplay between electron-electron Coulomb repulsion, charge, spin and orbital degrees of freedom *and* chemistry. Unfortunately, because of the strong electron-electron interaction, the standard *ab-initio* band structure approaches do not work for these *strongly correlated* systems. Thus a full understanding of their properties is, at present, missing; the most striking example is that, even 20 years after the discovery, the microscopic mechanism behind high-temperature superconductivity is still unknown.

In this lecture I will introduce the modern approach to the electronic structure of strongly correlated materials. The outline of the lecture is the following. First I will explain why traditional methods fail for these systems and discuss the effects of electron-electron repulsion. In order to treat these effects, many-body methods (beyond mean field) are needed. While the full many-body Hamiltonian of the system cannot be solved, few-band models can now be studied. I will show how to construct small but *realistic* model Hamiltonians, extracting the parameters from *ab-initio* calculations. I will then illustrate how to solve these models with a recently developed many-body method, the dynamical mean-field theory.

# 2 From ab-initio to many-body model Hamiltonians

Solids are complex many-body systems made of electrons and nuclei. While the heavy nuclei usually form a lattice and for many purposes can be considered as classical point charges, the light electrons move very fast in the potential of the nuclei. The (electronic) Hamiltonian of such a many-body system can be written as

$$H = T + V_{\text{ext}} + \sum_{i < j} \frac{1}{|r_i - r_j|}, \quad (1)$$

where  $T$  is the kinetic energy,  $V_{\text{ext}}$  is the external potential, and the last term the electron-electron repulsion and where we adopted atomic units ( $e = m = \hbar = 1$ ). The Coulomb interaction is usually very large, and makes the theoretical description of the electronic structure (the solution of Hamiltonian Eq. (1)) a very difficult task. In the presence of such a two-body interaction, the motion of each electron is strongly dependent on the motion of all the others and it is in practice impossible to calculate the many-body wavefunction even of a single atom. As introduced in the first lecture by R. Zeller, in 1964 a way out from this problem was found: density functional theory (DFT). This theory shifted the focus from the many-body wavefunction to physical quantities, in particular the charge-density. Hohenberg and Kohn [2] proved that the total energy of an interacting system is a functional of the charge-density and that, in addition, the ground state charge density minimizes the total energy; soon after Kohn and Sham [3]

showed that an interacting system can be formally mapped onto an equivalent non interacting system. By minimizing the total energy for fixed particle numbers, they obtained the equations

$$\left[ -\frac{\nabla^2}{2} + V_{\text{eff}} \right] \Psi_i = \varepsilon_i \Psi_i, \quad (2)$$

with

$$V_{\text{eff}} = V_{\text{ext}} + \int \frac{n(r')}{r - r'} dr' + \frac{\delta E_{xc}[n(r)]}{\delta n(r)} = V_{\text{ext}} + V_{\text{H}} + V_{xc}, \quad (3)$$

and with the ground state density given by  $n(r) = \sum_i^N |\Psi_i(r)|^2$ . These equations describe a single electron in an effective potential,  $V_{\text{eff}}$ , the sum of an external potential,  $V_{\text{ext}}$ , an electrostatic (Hartree) term  $V_{\text{H}}$ , and an additional *exchange-correlation* term,  $V_{xc}$ . The Kohn-Sham equations are a tremendous simplification of the original many-body problem and still are in principle exact. In practice, however, only approximations to the exchange correlation contribution are known. Among those the local density approximation (LDA), proposed in the 70s [4], turned out to be very successful. The generalized gradient approximation (GGA) is also used very often in electronic structure calculations. With a given choice of the exchange-correlation potential the ground state energy and the electronic structure is obtained by solving self-consistently the Kohn-Sham equations. At present DFT (based on LDA or GGA) can be used to understand and predict the properties of many materials, to design new materials, handle very large many-particles systems and it is used in different fields, ranging from physics to chemistry, biology and geology. For this success the noble prize in chemistry was awarded to W. Kohn in 1998 [5].

The main success of DFT (LDA/GGA) is that, thanks to the Kohn-Sham equations, it let us think about complex many-body systems in terms of single particle orbitals ( $\Psi_i$ ) and single particle energies ( $\varepsilon_i$ ). Although the Kohn-Sham equations are *only* an auxiliary problem and the Kohn-Sham energies are *only* Lagrange parameters (except for the highest energy,  $\varepsilon_N$ , which gives, in principle, the ionization energy,  $\varepsilon_N = -I$ ), they have been used with success also to calculate quasiparticles masses, Fermi surfaces, and in general to *understand* the electronic structure of complex materials. The main weakness of DFT is, instead, that there is no systematic procedure for improving  $V_{xc}$  and that it is not entirely clear why LDA/GGA are so successful for many complex systems.

However, there are some systems for which DFT fails, even qualitatively. Since this is true for all of the known approximations of  $V_{xc}$  (LDA, GGA, ...), I will from now on refer to LDA results only. The systems for which LDA fails are those with localized d or f electrons: in these materials the electron-electron Coulomb repulsion is particularly strong and the one-electron picture, obtained from Kohn-Sham equations, does not apply. Among the *strongly correlated systems* there are many of the modern challenges: high-temperature superconducting cuprates, colossal magneto-resistance materials, Mott and charge transfer insulators and strongly correlated metals, heavy-Fermions and Kondo systems [1]. Mott insulators [6] are the most striking example of this failure. In LDA, a crystal with an odd number of valence electrons per cell has partially filled bands and it is therefore metallic. However, there are materials in this category which are, experimentally, paramagnetic insulators:  $\text{V}_2\text{O}_3$  or  $\text{CoO}$  are famous examples. The origin of this insulating behavior is the strong electron-electron Coulomb repulsion, poorly described by LDA. A *simple model* which is believed to properly describe this interaction is the so-called one-band Hubbard model

$$H = -t \sum_{\langle i,j \rangle \sigma} c_{i\sigma}^\dagger c_{j\sigma} + U \sum_i n_{i\uparrow} n_{i\downarrow} \equiv \hat{T} + \hat{U}. \quad (4)$$

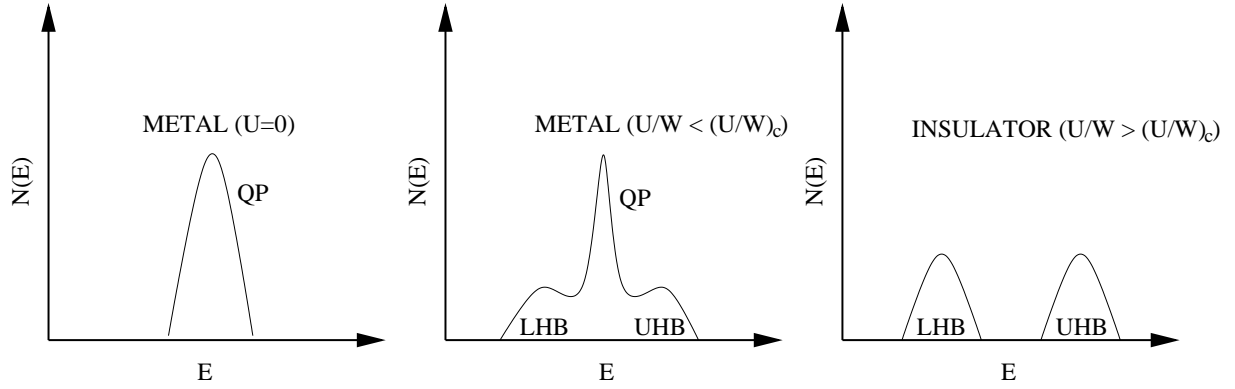


**Fig. 1:** Pictorial view of the metal-insulator transition. For  $U = 0$  the system is metallic; the spectral function  $N(E)$  shows a single feature, the quasi-particle peak. Increasing the ratio  $U/W$  the quasi-particle peak becomes progressively more narrow and some spectral weight is moved toward higher/lower energy; two broad features appear, the so-called lower (LHB) and upper (UHB) Hubbard bands. For larger  $U/W$  the system eventually becomes an insulator: the quasiparticle peak disappears and only the Hubbard bands are left.

Here  $t$  is the hopping integral from site  $i$  to its nearest neighbors  $j$ ,  $n_{i\sigma} = c_{i\sigma}^\dagger c_{i\sigma}$ ,  $c_{i\sigma}^\dagger$  ( $c_{i\sigma}$ ) creates (destroys) an electron with spin  $\sigma$  at site  $i$ , and  $U$  is the on-site Coulomb repulsion. If  $U = 0$ , at half filling ( $n = 1$  electron per atom), the Hamiltonian (4) describes a half-filled metallic band with a band width  $W$ ; in the atomic limit ( $W = 0$ ) it describes an (insulating) collection of isolated atoms. In the general case the kinetic energy  $\hat{T}$  and the Coulomb repulsion  $\hat{U}$  will compete: For  $U/W \ll 1$  (weak Coulomb interaction or wide band) the system is metallic; increasing  $U$  the quasi-electrons become progressively more heavy, and for  $U/W > (U/W)_c \sim 1$  the system is an insulator. No single-electron theory can describe such a Mott *metal-insulator* transition. The solution of the *simple* one-band Hubbard model, Eq. (4), already requires the fool-blown machinery of non-perturbative quantum many-body methods, and, apart from very special cases, can be still be achieved only within some approximation. A schematic picture of the Mott transition is displayed in Fig. 1.

Very recently a new and successful many-body tool was developed, the dynamical mean-field theory (DMFT) [7, 8]. In this approach the lattice Hubbard model is mapped into an effective single-site quantum impurity model, the parameters of which are found self-consistently. DMFT is a mean field method; differently than in traditional mean field techniques, however, in DMFT the (local) *dynamical fluctuations* are fully taken into account; only spatial fluctuations are frozen. Using the dynamical mean-field theory, the phase diagram of the Hubbard model could be studied in detail [8].

The self-consistent DMFT cycle requires, in each iteration, the solution of a *quantum impurity model*. For this purpose several many body approaches, some rigorous (e.g. quantum Monte Carlo and exact diagonalization), some approximate (e.g. iterative perturbation theory or the non crossing approximation) are used. Here we will focus only on one scheme, the scheme based on quantum Monte Carlo (QMC) [9]. With this numerically exact method, already the solution of a simple one-band model at high (1000 K) temperatures takes significant time on a normal workstation. For realistic problems (many orbitals, lower temperature) the computational effort increases substantially; to solve the full many-body Hamiltonian (1) is totally impossible. Only the most advanced parallel supercomputers presently start to make realistic

Hubbard models accessible. It is therefore fundamental to construct minimal models, in which only the strongest interactions and the most important states are retained. This conclusion is general, i.e., it is valid not only for the QMC scheme but also for all the other rigorous schemes. Exact diagonalization is, for example, limited by the prohibitive size of the Hilbert space, and therefore by the memory; again, while few-band models are accessible, complex many-orbital systems become easily out of reach.

The LDA electronic structure of most transition metal oxides exhibits few partially filled and narrow d bands: high temperature superconducting cuprates have a half-filled  $x^2-y^2$  band at the Fermi level, manganites have partially filled  $e_g$  states, several correlated metals and Mott insulators have partially filled  $t_{2g}$  or  $e_g$  bands. It is therefore natural to use generalized few-band Hubbard model for describing the low temperature properties of these materials. Such a model may be written as

$$H = - \sum_{im,jm',\sigma} t_{im,jm',\sigma} c_{im,\sigma}^\dagger c_{jm',\sigma} + \frac{1}{2} \sum_{imm'\sigma \neq \sigma'} U_{mm'} n_{im,\sigma} n_{im',\sigma'} + \frac{1}{2} \sum_{m \neq m',\sigma} (U_{mm'} - J_{mm'}) n_{im,\sigma} n_{im',\sigma} \quad (5)$$

Here  $t_{im,jm',\sigma}$  is the hopping integral between site orbital  $m$  on site  $i$  and orbital  $m'$  on site  $j$ . The electron-electron repulsion is a *local* (on-site) interaction, the sum of a direct and exchange term; for reasons that will be explained later we neglected the spin-flip terms in the exchange interaction.

The model Hamiltonian (5) has many *free* parameters: all the hopping integrals and the Coulomb couplings. It is therefore necessary to calculate as many of these parameters as possible from first principles. To date this is still a problem for the interaction terms, while the hoppings, which determine the chemistry of the material, can be reliably determined. In the next section I will show how they can be derived ab-initio by means of Wannier functions.

### 3 Realistic many-body models from LDA

#### 3.1 From the Bloch to the Wannier representation

In strongly correlated transition metal oxides, the difference among materials and the microscopic origin of exotic phenomena can be understood only if Coulomb repulsion and chemistry are treated on the same footing. Simple model Hamiltonians can easily overlook the non trivial part of the material dependence; they could be oversimplified, the parameters chosen could be unrealistic, and thus they can easily lead to wrong conclusions.

A strategy to construct realistic models is to extract the parameters from band structure calculations. Electronic structure techniques solve the Kohn-Sham equation for a given approximation of the exchange potential and for a periodic system

$$\left[ -\frac{\nabla^2}{2} + V_{\text{eff}}(\mathbf{r}) \right] \Psi_{\mathbf{k}}^i = \varepsilon_i(\mathbf{k}) \Psi_{\mathbf{k}}^i. \quad (6)$$

As a result, they yield the energy bands  $\varepsilon_i(\mathbf{k})$  and the corresponding Bloch functions,  $\Psi_{\mathbf{k}}^i(\mathbf{r})$ . LDA electronic structures are, in general, very complicated to analyze, since they can extend

over several Rydbergs and can include, depending on the method used for solving the Kohn-Sham equations, up to thousands basis functions. Electronic structure techniques based on minimal local basis sets (like the Linear Muffin Tin Orbital (LMTO) method) produce smaller matrices and are more accessible to a physical interpretation. Still, it is difficult to disentangle the relevant parameters from the full LDA band structure. Thus, in order to construct many-body models, Wannier functions became recently very popular and have already proven to be quite powerful. Formally, a Wannier function is obtained as a Fourier transform of the Bloch functions,  $\Psi_{\mathbf{k}}^i(\mathbf{r})$ ,

$$w_{\mathbf{T}}^i(\mathbf{r}) = \frac{\Omega}{8\pi^3} \int d\mathbf{k} \Psi_{\mathbf{k}}^i(\mathbf{r}) \exp(-i\mathbf{k} \cdot \mathbf{T}), \quad (7)$$

where  $\Omega$  is the volume of the primitive cell, the integral is extended to the first Brillouin zone and  $\mathbf{T}$  is a reciprocal lattice vector.

The Wannier function for a given band is not unique, because the Bloch function can be multiplied by an arbitrary phase factor; consequently there are different methods for obtaining Wannier functions from LDA calculations. A very efficient approach is the downfolding technique based on the recently developed  $N^{\text{th}}$ -order Muffin Tin Orbital method (NMTO) [10] which I will describe in the next section; the NMTO Wannier functions, the localization of which is assured through the choice of boundary conditions, provide direct insight into the chemistry of materials. Other techniques of constructing Wannier functions exploit the arbitrariness of the phase and minimize the spread (defined with a given, but essentially arbitrary, criterium) of the Wannier functions [12]; these techniques, developed for plane-wave based methods, have been exported also to other band structure methods [16].

For strongly correlated systems, Wannier functions, if sufficiently localized, are the ideal building blocks for constructing (from first principles) generalized Hubbard models; Wannier functions yield directly the real space Hamiltonian, i.e., hopping integrals and on-site energies for the bands they span.

### 3.2 Electronic structure calculations with the NMTO method

NMTO is a special technique to solve the Kohn-Sham equation in a periodic potential. To solve this equation, space is divided into spatially separate regions (overlapping spheres of radius  $s_R$ , centered on the atoms, and interstitial regions); the Kohn-Sham (or Schrödinger) equation is solved in each region separately and only at the end the solutions are matched at the interface. Close to the nuclei (inside the atoms) the potential changes rapidly ( $\sim 1/r$ ) with the distance, while in the interstitial regions between the atoms it varies more slowly. Furthermore, free atoms are spherical and, to good approximation, they remain almost spherical in solids, in particular close to their nucleus. Thus the potential can be approximated with a superposition of spherically symmetric (atomic-like) potentials,  $v_R$ , with range  $s_R$  and a constant interstitial potential (Muffin Tin approximation)

$$V_{\text{eff}} = \sum_R v_R(\mathbf{r} - \mathbf{R}) \Theta(|\mathbf{r} - \mathbf{R}| - s_R) + V_{\text{intz}} \Theta_I(\mathbf{r}), \quad (8)$$

where  $\Theta$  is the step function and  $\Theta_I = 1 - \sum_R \Theta(|\mathbf{r} - \mathbf{R}| - s_R)$ .

Inside a sphere, the Schrödinger equation may be written as [13]

$$-\frac{1}{2r} \left[ \frac{\partial^2}{\partial r^2} r \varphi_{\varepsilon, Rl}(r) - \frac{l(l+1)}{r} r \varphi_{\varepsilon, Rl}(r) \right] Y_L + v_R(r) \varphi_{\varepsilon, Rl}(r) Y_L = \varepsilon \varphi_{\varepsilon, Rl}(r) Y_L, \quad (9)$$

where  $Y_L$  is a spherical harmonic with quantum numbers  $L = lm$ . The regular solutions of (9) for a chosen energy and momentum are the *partial waves*,

$$\varphi_{RL}(\varepsilon_n, \mathbf{r}_R) = \varphi_{\varepsilon_n, RL} Y_L, \quad (10)$$

where  $\mathbf{r}_R = \mathbf{r} - \mathbf{R}$ . In the NMTO method the partial waves are calculated for a set of energies  $\varepsilon_n = \varepsilon_0, \dots, \varepsilon_N$ . Next, hard spheres are constructed around each atom; hard spheres have a radius  $a_R$  and, differently from the potential spheres, they do *not* overlap. The Schrödinger equation is then solved in the (empty) interstitial region, where it can be written as

$$\nabla^2 \psi = -(\varepsilon - V_{\text{mtz}}) \psi = -k^2 \psi. \quad (11)$$

There are different ways of solving Eq. (11). Here the solutions – the *screened spherical waves* – are expressed as a superpositions of spherical Hankel functions. Furthermore, the screened spherical wave centered at site  $\mathbf{R}$  and of character  $L$ ,  $\psi_{RL}(\varepsilon_n, |\mathbf{r} - \mathbf{R}|)$ , is constructed with the following boundary conditions

$$\psi_{RL}(\varepsilon, |\mathbf{r} - \mathbf{R}| = a_{\mathbf{R}'}) = \begin{cases} Y_L & \text{if } \mathbf{R}' = \mathbf{R}; \\ 0 & \text{if } \mathbf{R}' \neq \mathbf{R}. \end{cases} \quad (12)$$

This means that the screened spherical wave — by construction — vanishes on all the hard spheres except its own, where it equals the spherical harmonic  $Y_L$ . The above choice of the boundary conditions helps in matching the interstitial solution to the partial waves and assures the localization of the NMTOs. To compute the screened spherical wave is usually the major task in an NMTO calculation.

At this point we can match the solutions in the different regions and construct the *kinked partial waves*, linear combinations of a partial wave and a screened spherical wave. The kinked partial wave,  $\phi_{RL}(\varepsilon, |\mathbf{r} - \mathbf{R}|)$  is, by construction, a solution of the Schrödinger equation in all space except at the hard spheres, where it has a kink. The true solution is the linear combination  $|\Psi\rangle = \sum_{RL} c_{RL} |\phi_{RL}\rangle$  of kinked partial waves for which the kinks cancel. The kink-cancellation condition leads to the secular equation

$$K(\varepsilon) \cdot \mathbf{c} = 0. \quad (13)$$

This equation is also known as the screened Korringa-Kohn-Rostoker (KKR) secular equation and  $K(\varepsilon)$ , the kink-matrix, is the screened KKR matrix [11]. In KKR the non-zero solutions of the linear homogeneous Eq. (13) give directly the eigenvalues  $\varepsilon_i$ . Another possibility to obtain eigenvectors and eigenvalues is the linearization approach which is at the basis of the successes of the LMTO method or the polynomial interpolation used in the NMTO method. Let's see how the linearization works. The first order Taylor expansion of the KKR matrix around the energy  $\varepsilon_\nu$  yields

$$\langle \Psi | K(\varepsilon) | \Psi \rangle = 0 \sim K(\varepsilon_\nu) + (\varepsilon - \varepsilon_\nu) \dot{K}(\varepsilon_\nu) + \dots, \quad (14)$$

and the corresponding expansion of the wave function is

$$|\Psi\rangle = |\phi(\varepsilon_\nu)\rangle + (\varepsilon - \varepsilon_\nu) |\dot{\phi}(\varepsilon_\nu)\rangle + \dots \quad (15)$$

Solving the secular equation at *zero order* ( $|\psi\rangle = |\phi(\varepsilon_\nu)\rangle$ ) leads to the generalized eigenvalue problem defined by the Hamiltonian and overlap

$$\langle \phi(\varepsilon_\nu) | H - \varepsilon_\nu | \phi(\varepsilon_\nu) \rangle = -K(\varepsilon_\nu), \quad \langle \phi(\varepsilon_\nu) | \dot{\phi}(\varepsilon_\nu) \rangle = \dot{K}(\varepsilon_\nu). \quad (16)$$

At this point, it is useful to introduce the set of Muffin Tin Orbitals (MTO)

$$|\chi(\varepsilon)\rangle = |\phi(\varepsilon)\rangle - |\dot{\phi}(\varepsilon_\nu)\rangle \dot{K}^{-1}(\varepsilon_\nu) K(\varepsilon). \quad (17)$$

The MTOs are a complete basis with respect to the Muffin Tin potential, because a given solution of the KKR equation,  $|\Psi\rangle = |\phi(\varepsilon_j)\rangle \mathbf{c}_j$ , can be expressed as  $|\chi(\varepsilon_j)\rangle \mathbf{c}_j = |\phi(\varepsilon_j)\rangle \mathbf{c}_j = |\Psi\rangle$ , with the same coefficients; the MTO is independent of energy to linear order, because  $|\dot{\chi}(\varepsilon_\nu)\rangle = 0$ . We can use the MTOs to calculate the effective Hamiltonian and overlap to any order. In order to do this we use the following results, which hold for the kinked partial waves

$$\langle \phi(\varepsilon_\nu) | \phi(\varepsilon_\nu) \rangle = \dot{K}(\varepsilon_\nu) \quad \langle \phi(\varepsilon_\nu) | \dot{\phi}(\varepsilon_\nu) \rangle = \ddot{K}(\varepsilon_\nu)/2! \quad \langle \dot{\phi}(\varepsilon_\nu) | \dot{\phi}(\varepsilon_\nu) \rangle = \ddot{K}(\varepsilon_\nu)/3!. \quad (18)$$

In the MTO basis, the *first order* solution of the secular equation (13) is therefore

$$\langle \chi^{(1)}(\varepsilon_\nu) | H - \varepsilon_\nu | \chi^{(1)}(\varepsilon_\nu) \rangle = -K(\varepsilon_\nu) + K(\varepsilon_\nu) \dot{K}^{-1}(\varepsilon_\nu) \frac{\ddot{K}(\varepsilon_\nu)}{2!} \dot{K}^{-1}(\varepsilon_\nu) K(\varepsilon_\nu), \quad (19)$$

with the overlap

$$\begin{aligned} \langle \chi^{(1)}(\varepsilon_\nu) | \chi^{(1)}(\varepsilon_\nu) \rangle &= \dot{K} - K(\varepsilon_\nu) \dot{K}^{-1} \frac{\ddot{K}(\varepsilon_\nu)}{2!} - \frac{\ddot{K}(\varepsilon_\nu)}{2!} \dot{K}^{-1}(\varepsilon_\nu) K(\varepsilon_\nu) \\ &+ K(\varepsilon_\nu) \dot{K}^{-1}(\varepsilon_\nu) \frac{\ddot{K}(\varepsilon_\nu)}{3!} \dot{K}^{-1}(\varepsilon_\nu) K(\varepsilon_\nu). \end{aligned} \quad (20)$$

The first order MTOs,  $|\chi^{(1)}(\varepsilon_\nu)\rangle$ , correspond to a set of LMTOs, they are, however, complete to linear order with respect to the Hamiltonian and yield eigenvalues correct up to fourth order. The NMTO method is a generalization of this. Now the solution of the Schrödinger equation is obtained by means of a polynomial interpolation of the true solution; therefore the NMTOs span the space of the true solutions  $\Psi_i(\varepsilon_i, \mathbf{r})$  with an error of order  $\propto (\varepsilon_i - \varepsilon_0) \dots (\varepsilon_i - \varepsilon_N)$ . The set of NMTOs can be written as

$$\chi_{RL}^{(N)}(\mathbf{r}) = \sum_{n=0}^N \sum_{R'L'} \phi_{R'L'}(\varepsilon_n, \mathbf{r}) L_{n;R'L',RL}^N \quad (21)$$

where  $L_n^N$  are coefficients in the Lagrange interpolation formula. In the limit where all the energies  $\varepsilon_0 \dots \varepsilon_N$  are identical to  $\varepsilon_\nu$  these coefficients can be expressed as a function of  $G(\varepsilon) = K^{-1}(\varepsilon)$  and its energy derivatives. It can be shown that the NMTO Hamiltonian can then be expressed as

$$\langle \chi^{(N)} | H - \varepsilon_\nu | \chi^{(N)} \rangle = - \left( \frac{G^{(N)}}{N!} \right)^{-1} \left( \frac{G^{(2N)}}{2N!} \right) \left( \frac{G^{(N)}}{N!} \right)^{-1}, \quad (22)$$

where  $G^{(N)}$  is the  $N^{th}$  energy derivative of  $G$ ; in a similar way the overlap can be written as

$$\langle \chi^{(N)} | \chi^{(N)} \rangle = - \left( \frac{G^{(N)}}{N!} \right)^{-1} \left( \frac{G^{(2N+1)}}{2N+1!} \right) \left( \frac{G^{(N)}}{N!} \right)^{-1}. \quad (23)$$

Thus, in the limit of a condensed mesh, the  $N=1$  NMTO (two energies) yields the LMTO Hamiltonian and overlaps, Eq. (19) and Eq. (20).



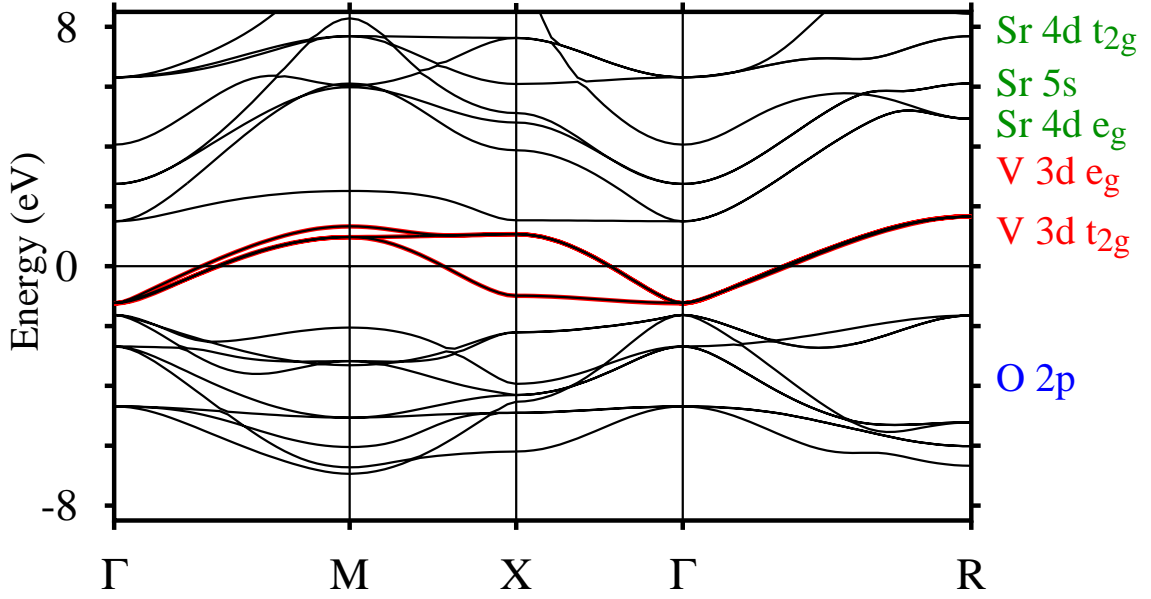


**Fig. 2:** The LDA electronic structure of  $\text{SrVO}_3$  obtained with the NMTO method. The black lines are the NMTO bands (full Hamiltonian). The red lines are the bands obtained by downfolding all the states but the  $t_{2g}$ ; the  $N+1$  energies used for the interpolation, measured with respect to the Fermi level, are  $\varepsilon_0 = 0.6$  eV,  $\varepsilon_1 = 0.2$  eV and  $\varepsilon_2 = 0.8$  eV. From Ref. [20].

The NMTO band energies are then obtained as the eigenvalues of the orthogonal Hamiltonian

$$H = \langle \chi^{(N)\perp} | H | \chi^{(N)\perp} \rangle, \quad (24)$$

where

$$|\chi^{(N)\perp}\rangle \equiv |\chi^{(N)}\rangle \langle \chi^{(N)} | \chi^{(N)} \rangle^{-1/2} \quad (25)$$

are symmetrically orthonormalized NMTO.

The NMTO Wannier basis for these bands can then be obtained by Fourier transform of the symmetrically orthonormalized NMTOs

$$\chi_{RL}^{(N)\perp}(\mathbf{r} - \mathbf{T} - \mathbf{R}) = \frac{\Omega}{8\pi^3} \int d\mathbf{k} \chi_{RL}^{(N)\perp}(\mathbf{k}, \mathbf{r}) \exp(-i\mathbf{k} \cdot (\mathbf{R} + \mathbf{T})). \quad (26)$$

The NMTO Wannier basis set yields the hopping integrals and the on-site energies.

Up to now we have considered all the channels active. However, in order to construct *minimal* many-body models, we need to disentangle the important degrees of freedom from all the rest. This is achieved by means of the downfolding procedure, described in the next session.

### 3.3 Downfolding and NMTO Wannier functions

Let's consider the cubic perovskite  $\text{SrVO}_3$ ; this system has a cubic primitive cell with V at (0,0,0), O at (1/2,0,0) and Sr at (1/2,1/2,1/2). Fig. 2 shows the electronic structure of this

material obtained with the NMTO method [19, 20]. We see that the O bands are totally filled, the V- $t_{2g}$  bands are filled by one electron, and the V- $e_g$  bands as well as the Sr bands are empty. Experimentally, this system is a strongly correlated metal with mass enhancement of  $\sim 2 - 3$ . The LDA band structure suggests that only (or mainly)  $t_{2g}$  electrons are involved in the low energy physics. It is therefore reasonable to think that a 3-band Hubbard model is the minimal model required to describe this system. In order to obtain the parameters of this model, the O-p, Sr-d, Sr-s and V- $e_g$  channels have to be integrated out: only the  $t_{2g}$  degrees of freedom can be retained. To do this we use the NMTO-based *downfolding* method. The channels are divided into passive (P) and active (A). For each active channel a kinked partial wave is constructed from all the partial waves and from a screened spherical wave; such a kinked partial wave has kinks only in the active channels, while it is smooth in the passive (or downfolded) channels. The NMTOs constructed from these partial waves can have passive-channel character both at their own site and at other sites, while the projection of the NMTOs on the active channels vanish at other sites. Thus the passive channels reshape the NMTOs and, in general, make the NMTOs longer range. It is important to notice that these NMTOs span a number of bands equal to the number of active channels; furthermore in order to span a given set of bands, the Bloch states which describe these bands should have sizable active-channel character; finally, the energies for the polynomial interpolation must be chosen within the targeted bands, as done in the example shown in Fig. 2.

The NMTO downfolding may look like a complicated procedure; it is therefore useful to compare it with the simpler Löwdin downfolding method. Let's start from the eigenvalue problem

$$\begin{pmatrix} H_{AA} & H_{AP} \\ H_{PA} & H_{PP} \end{pmatrix} \begin{pmatrix} c_A \\ c_P \end{pmatrix} = \varepsilon \begin{pmatrix} c_A \\ c_P \end{pmatrix} \quad (27)$$

and let's define the matrix  $K(\varepsilon) = -H + \varepsilon$ , so that the equation above can be rewritten as  $K(\varepsilon) \cdot \mathbf{c} = 0$ . Using the Löwdin procedure we can eliminate  $c_P$  and rewrite the Hamiltonian in the space of active channel A as follows

$$\tilde{H}_{AA} - \varepsilon = -K_{AA}(\varepsilon) + K_{AP}K_{PP}^{-1}(\varepsilon)K_{PA} \equiv -K_D(\varepsilon). \quad (28)$$

In a similar way, eliminating  $c_P$ , one can rewrite the wavefunction as

$$|\Psi(\varepsilon)\rangle = |\phi_D(\varepsilon)\rangle = |\phi_A\rangle c_A + |\phi_P\rangle c_P = |\phi_A\rangle c_A - |\phi_P\rangle K_{PP}^{-1}(\varepsilon)K_{PA}c_A$$

This Hamiltonian and the wavefunction depend on energy; in order to obtain the eigenvectors and the eigenvalues, the energy dependent term is usually approximated to linear order around some energy  $\varepsilon_\nu$ , e.g. the Fermi level or the center of the active channel bands; this leads to the generalized eigenvalues problem defined by the Hamiltonian and the overlap

$$H_{AA} - \varepsilon_\nu = -K_D(\varepsilon_\nu), \quad O_{AA} = \dot{K}_D(\varepsilon_\nu). \quad (29)$$

Similarly, one can also obtain the first order wavefunction

$$|\Psi(\varepsilon_\nu)\rangle = |\phi_D(\varepsilon_\nu)\rangle - |\dot{\phi}_D(\varepsilon_\nu)\rangle \dot{K}_D^{-1}(\varepsilon_\nu)K_D(\varepsilon_\nu). \quad (30)$$

Although Löwdin downfolding is often used, the energy bands obtained with the linear approximation are usually only a poor approximation of the original the LDA bands, especially if massive downfolding (from LDA to one or few bands) is required. The NMTO downfolding works in a similar way as the Löwdin procedure, but reduces the error in the wavefunction to

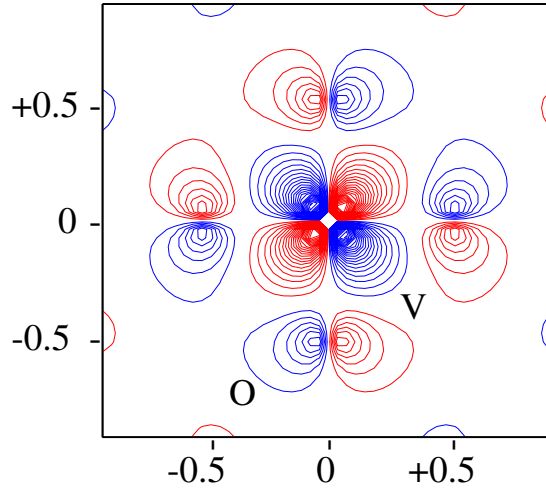


**Fig. 3:** *SrVO<sub>3</sub>: The xy-NMTO real-space orbital (before orthogonalization) in the xy-plane. The orbital was obtained by downfolding all the channels but the  $t_{2g}$ . The V is at the center, the O are located at  $(\pm 1/2, 0)$ ,  $(0, \pm 1/2)$ .*

order  $N$ . The  $\text{SrVO}_3$ - $t_{2g}$  bands obtained by downfolding all channels but the  $t_{2g}$  are displayed in red in Fig. 2: we see that these bands (obtained with  $N+1=3$  energies) are basically identical to the original LDA bands.

In order to better explain how downfolding works in practice, we simplify the  $\text{SrVO}_3$  Hamiltonian neglecting the Sr states and adopting a tight binding (TB) approximation for O-p and V-d states. The aim is to eliminate the filled O-p states, the empty  $e_g$  states and only retain the  $t_{2g}$  states. First we notice that, in the TB approximation, since  $\text{SrVO}_3$  is a cubic perovskite each V-d state is coupled only to two O-p states, different for each d orbitals. Thus the Hamiltonian for the, let's say, xy-orbitals will look like (in  $\mathbf{k}$  space)

H	$ \phi_{Vxy}(\mathbf{k})\rangle$	$ \phi_{O1x}(\mathbf{k})\rangle$	$ \phi_{O2y}(\mathbf{k})\rangle$
$\langle\phi_{Vxy}(\mathbf{k}) $	$\varepsilon_d$	$-2t_{pd} \sin k_y/2$	$-2t_{pd} \sin k_x/2$
$\langle\phi_{O1x}(\mathbf{k}) $	$-2t_{pd} \sin k_y/2$	$\varepsilon_p$	0
$\langle\phi_{O2y}(\mathbf{k}) $	$-2t_{pd} \sin k_x/2$	0	$\varepsilon_p$

Downfolding the O orbitals with the Löwdin procedure, the energy-dependent Hamiltonian and overlap

$$\tilde{H}(\varepsilon) - \varepsilon = \varepsilon_d + \frac{4t_{pd}^2}{\varepsilon - \varepsilon_p} - \frac{4t_{pd}^2}{\varepsilon - \varepsilon_p}(\cos k_x + \cos k_y) = -K_D(\varepsilon), \quad O = \dot{K}_D(\varepsilon)$$

can be obtained. In addition, the Bloch function for the xy-orbital may be written as

$$|\phi_{Dxy}(\mathbf{k})\rangle = |\phi_{xy}(\mathbf{k})\rangle + \frac{2t_{pd} \sin k_x/2}{\varepsilon - \varepsilon_p} |\phi_{O1x}(\mathbf{k})\rangle + \frac{2t_{pd} \sin k_y/2}{\varepsilon - \varepsilon_p} |\phi_{O2y}(\mathbf{k})\rangle. \quad (31)$$

In the linear approximation

$$|\phi_{Dxy}(\varepsilon_\nu)\rangle = |\phi_{xy}(\varepsilon_\nu)\rangle - |\dot{\phi}_{xy}(\varepsilon_\nu)\rangle \dot{K}_D^{-1}(\varepsilon_\nu) K_D(\varepsilon_\nu).$$

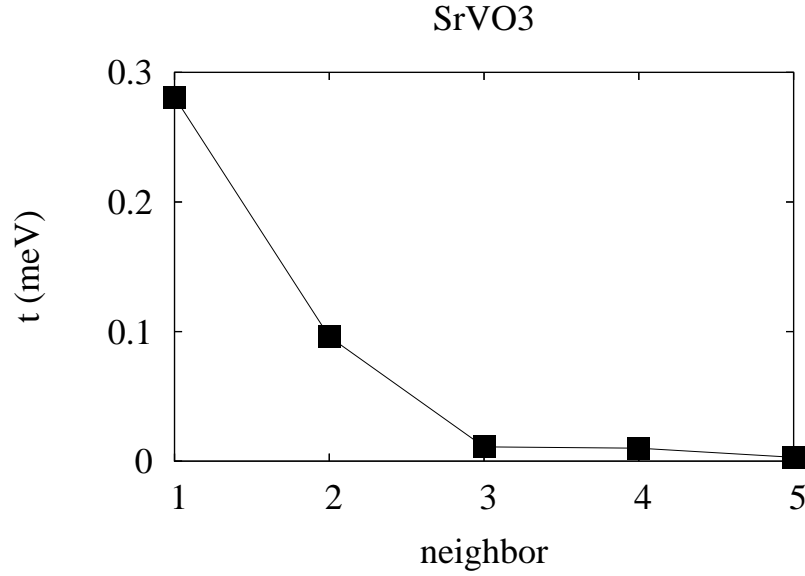


**Fig. 4:** *Hopping integrals vs. neighbors in SrVO<sub>3</sub> for the xy-Wannier functions. Only the neighbors in the xy-plane are considered. The values are taken from Ref. [20].*

Eq. (31) shows that the downfolded wavefunction has tails on the O-sites, which is what we also see in the NMTO Wannier function Fig. 3. Again, the linear approximation yields a poor expression of the eigenvectors. In the NMTO the wavefunction is of order  $N$  and the error is  $\propto c^{(N)}(\varepsilon_i - \varepsilon_0) \dots (\varepsilon_i - \varepsilon_N)$ , where the constant  $c^{(N)}$  depends on the size of the set and it is larger the smaller the set is. Clearly, the larger the number of downfolded orbitals, the smaller is the energy window over which the bands are correctly reproduced, the more important is to go beyond the linear approximation; in addition, since their interpolation error is different, the downfolded NMTOs and the original ones are not equivalent although they both span the, e.g.,  $t_{2g}$  bands.

We obtained Eq. (30) by using the Löwdin procedure. The expression for the downfolded NMTO is — in the general case — rather complicated. In the limit of a condensed mesh, however, in the linear approximation the downfolded N=1 NMTO,  $|\chi_D(\varepsilon_\nu)\rangle$ , can be written as (30); in this case  $|\Psi(\varepsilon_\nu)\rangle = |\chi_D(\varepsilon_\nu)\rangle$ ,  $K_D$  is the downfolded kink-matrix,  $K_D(\varepsilon) = K_{AA}(\varepsilon) + K_{AP}(\varepsilon)K_{PP}^{-1}(\varepsilon)K_{PA}(\varepsilon)$  and  $|\phi_D(\varepsilon)\rangle$  a downfolded partial wave, defined as

$$|\phi_D(\varepsilon)\rangle = |\phi_A(\varepsilon)\rangle - |\phi_P(\varepsilon)\rangle K_{PP}^{-1}(\varepsilon) K_{PA}(\varepsilon). \quad (32)$$

### 3.4 Wannier functions as a basis for the Hubbard model

The Fourier transform of the downfolded (symmetrically orthogonalized) NMTO Hamiltonian yields hopping integrals and on-site energies; in a similar way the Fourier transform of the (symmetrically orthogonalized) NMTOs yields a set of NMTO Wannier functions. These Wannier functions can be used as a basis for the many-body Hamiltonian, i.e., the generalized Hubbard model, Eq. (5). There are several approximations behind using LDA Wannier functions (constructed with the NMTO or other methods) as correlated electrons. In this section I will discuss some of them.

First, in the Hubbard model, Eq. (5), the Coulomb interaction is local (on-site). This is reasonable for the localized atomic  $d$  states; Wannier functions are, however, longer-ranged than atomic  $d$  wave-functions, and the validity of this approximation depends therefore on their degree of localization. Thus it is important, for a given set of Wannier functions, to know how small the long range Coulomb terms are compared to the on-site interaction. While it is not clear, at present, how to construct the Wannier functions which best satisfy this requirement, the localization of NMTO Wannier functions is assured by the choice of boundary conditions used in constructing the screened spherical waves. Downfolding delocalizes the Wannier orbitals. Nevertheless, before orthogonalization, the NMTO cannot, by construction, have active channel character on other sites and it is therefore unlikely that the Coulomb repulsion in the Wannier basis is long-ranged. This can be seen in Fig. 3 for the  $xy$ -orbital in  $\text{SrVO}_3$ : the orbital has O- $p$  but no V- $xy$  tails. Orthogonalization introduces however (small) longer-ranged  $xy$  tails. In the case of  $\text{SrVO}_3$  Figure 4 shows that, for this material, despite both massive downfolding and orthogonalization, hopping integrals decay very rapidly after the second neighbors, an indication of a rather strong localization. Of course the actual degree of localization depends on the orbital and on the system, and has to be verified case by case;  $e_g$  orbitals hybridize more strongly with O than  $t_{2g}$  orbitals, and therefore, for transition metal oxides with partially filled  $e_g$  states (such as  $\text{LaMnO}_3$ ), downfolding the O- $p$  states, usually has a bigger impact on the extent of the Wannier functions than for the  $t_{2g}$  systems.

A second important point is that LDA Wannier functions are constructed by downfolding one-electron states. This is different from downfolding the many-body Hamiltonian, an operation that would lead, in general, to complex effective Hamiltonians with, e.g., three- or higher-body interactions. The Hubbard Hamiltonians constructed from LDA Wannier functions do not carry any information on such kind of many-body terms. A simple example: for  $\text{SrVO}_3$  we downfolded (one-electron downfolding) the empty  $e_g$  channels. Clearly, we are neglecting all the effects of the  $t_{2g}$ - $e_g$  Coulomb repulsion; in reality this repulsion is, most likely, of the same order of magnitude as the  $t_{2g}$ - $t_{2g}$  Coulomb interaction. If  $t_{2g}$ - $e_g$  fluctuations become important in some temperature regimes and/or for some specific properties, the  $t_{2g}$  Hubbard model is insufficient. There is no systematic way to know *a priori* how important, in a given basis, the neglected terms are for the low temperature-properties of a given system, and in most of the cases it can only be verified afterwards.

Finally, the effect of the Coulomb interaction of the downfolded channels is included as a renormalization (*screening*) of the Coulomb integrals. Before downfolding (i.e. for the full Hamiltonian (1)) the Coulomb interaction is exactly given by the bare Coulomb integrals for the Wannier functions, e.g., the direct- and exchange-Coulomb integral would then simply be

$$U_{mm'} = \left\langle mm' \left| \frac{1}{r_{12}} \right| mm' \right\rangle, \quad (33)$$

$$J_{mm'} = \left\langle mm' \left| \frac{1}{r_{12}} \right| mm' \right\rangle, \quad (34)$$

in a given Wannier basis set. The elimination of many states, however, makes the problem of calculating  $U$  very hard, because all the eliminated states contribute to screen the electron-electron repulsion. At present there is no reliable way of calculating the screened Coulomb interaction in a given basis, although different methods have been proposed and are used [18]. Thus  $U_{mm'}$  and  $J_{mm'}$  essentially remain free parameters and have to be obtained empirically, e.g., by the analysis of trends in series of similar materials.

## 4 DMFT solution of realistic many-body models

### 4.1 Dynamical mean-field theory

In this session we discuss how to solve a generalized Hubbard model with dynamical mean field theory (DMFT) [7, 8]. The Hubbard model is very complicated because it describes a *lattice* of strongly correlated electrons. In DMFT this *lattice* problem is replaced by an effective *single-site quantum impurity model* (e.g. the Anderson model) embedded in an effective medium (the so-called bath), the parameters of which are determined through a self-consistent procedure. DMFT is a generalization of the static mean field theory used in statistical mechanics. It is *dynamical* because it takes into full account local quantum fluctuations, i.e. temporal fluctuation of the number of electrons at a given site. It is *local* because spatial fluctuations are frozen; thus the self-energy depends on the frequency but it does not depend on the  $\mathbf{k}$  vector

$$\Sigma(\mathbf{k}, \omega) \sim \Sigma(\omega). \quad (35)$$

This is exact in infinite dimensions [7], but in realistic cases it is an approximation. Nevertheless, DMFT is a very powerful tool to study strongly correlated metals and the Mott metal-insulator transition, and more in general all kind of phenomena in which time fluctuations are the key ingredient. A review of the early successes of DMFT is reported in Ref. [8].

The strength of DMFT is the simplification introduced mapping a lattice problem in a single impurity model; still the effective quantum impurity model remains a many-body model and it has to be solved with an appropriate many-body technique. There are many possible methods or *impurity solvers* which are commonly used at this purpose [8]. As already anticipated, here I will only present the scheme based on quantum Monte Carlo (QMC).

In this scheme, the single impurity model is solved on the imaginary time axis. We will call  $G$  the impurity Green function and  $\mathcal{G}_0$  the bath Green function.

The local Green function  $G$  is given by

$$G(\tau) = \sum_n \exp(-i\omega_n \tau) \int d\varepsilon \frac{N(\varepsilon)}{i\omega_n + \mu - \varepsilon - \Sigma(i\omega_n)} \quad (36)$$

where  $N(\varepsilon)$  is the  $U = 0$  density of states,  $\mu$  is the chemical potential,  $\Sigma(i\omega_n)$  is the local self-energy (zero in the first iteration),  $\omega_n$  are the Matsubara frequencies,  $\omega_n = (2n + 1)\pi/\beta$ , with  $\beta = 1/k_B T$ . The bath Green function is obtained from  $G$  and  $\Sigma$  through the equation

$$\mathcal{G}_0^{-1} = G^{-1} + \Sigma. \quad (37)$$

$\mathcal{G}_0$ , together with the Coulomb terms, are then used to construct the effective quantum impurity model, described by the effective action

$$S_{\text{eff}} = - \int_0^\beta d\tau \int_0^\beta d\tau' \sum_\sigma c_\sigma^\dagger(\tau) \mathcal{G}_0^{-1}(\tau - \tau') c_\sigma(\tau') + U \int_0^\beta d\tau n_\uparrow(\tau) n_\downarrow(\tau). \quad (38)$$

This effective single site model is then solved with the Hirsch-Fye QMC algorithm [9]. The key steps are the following. First the imaginary time is discretized into  $L$  slices of size  $\Delta\tau = \beta/L$ ; consequently, the action is also discretized. The partition function is then obtained by using the Trotter decomposition

$$\exp(-\Delta\tau \hat{T} - \Delta\tau \hat{U}) \sim \exp(-\Delta\tau \hat{T}) \exp(-\Delta\tau \hat{U}), \quad (39)$$

where  $\hat{T}$  is the kinetic and  $\hat{U}$  the Coulomb repulsion term of the effective model. Second, the quartic terms in the action (due to  $\hat{U}$ ) are decoupled by means of a Hubbard-Stratonovich transformation

$$\exp(-\Delta\tau U n_{\uparrow} n_{\downarrow} + (\Delta\tau U/2)(n_{\uparrow} + n_{\downarrow})) = \frac{1}{2} \exp(\lambda s(n_{\uparrow} - n_{\downarrow})), \quad (40)$$

and  $\lambda = \text{arccosh}[\exp(\Delta\tau U/2)]$ . The variable  $s$  is a Ising field ( $s = \pm 1$ ); this transformation is performed at every time slice, and therefore  $s_1 \dots s_L$  Ising variables are introduced. This leads to the following relation

$$G_{\sigma}^{-1} = \mathcal{G}_{0\sigma}^{-1} \exp(V) + \exp(V) - 1 \quad (41)$$

where  $V = \exp(\sigma \lambda s_{\tau})$ . The partition function becomes

$$Z = \sum_{s_1 \dots s_L} \det[G_{\uparrow}(s_1, \dots, s_L)] \det[G_{\downarrow}(s_1, \dots, s_L)] \quad (42)$$

and the interacting Green function

$$G_{\sigma} = \frac{1}{Z} \sum_{s_1 \dots s_L} \det[G_{\uparrow}(s_1, \dots, s_L)] \det[G_{\downarrow}(s_1, \dots, s_L)] G_{\sigma}(s_1, \dots, s_L).$$

The interacting (impurity) Green function  $G$  is then obtained by stochastic Monte Carlo sampling, using  $\det[G_{\uparrow}(s_1, \dots, s_L)] \det[G_{\downarrow}(s_1, \dots, s_L)]$  as a stochastic weight. When a move is accepted the Green function is updated. The following Dyson equation

$$G' = \mathcal{A}^{-1}G, \quad \mathcal{A} = 1 + (1 - G)[\exp(V) - \exp(V')], \quad (43)$$

which relates any couple of Ising spin configurations, should in principle be used for updating  $G$  (*clean update*). The inversion of the  $L \times L$  matrix  $\mathcal{A}$  is, however, very time consuming; in practice, an approximate formula, the so-called *dirty update*, is used for most updates, and only few times the clean update Eq. (43) is actually used. At the end of the QMC simulation, the impurity Green function  $G$  is obtained; the new self energy is then calculated from Eq. (37). At this point the self-energy can be used in Eq. (36) to obtain  $G$  and then calculate the new bath Green function; the procedure continues till self-consistency in the self-energy is reached. Usually 10-15 iterations are necessary.

The output of a DMFT simulation is the green function  $G$  on the imaginary time axis. The spectral function

$$A(\omega) \equiv \frac{1}{\pi} G(\omega + i0) \quad (44)$$

on the real axes is obtained from the converged  $G(\tau)$  by analytical continuation. The standard algorithm used is the maximum entropy method [14]. It is important to notice, that with this technique, the spectral function is extracted from the Laplace transform

$$G(\tau) = \int_{-\infty}^{\infty} d\omega \frac{\exp(-\tau\omega)}{1 + \exp(-\beta\omega)} A(\omega),$$

i.e. solving an ill-posed problem; in order to obtain reliable spectral functions the statistical errors of  $G(\tau)$  must be very small and properly kept into account.

We point out that, in this DMFT scheme, the computational demanding task is the numerical solution of the single impurity problem by means of QMC. The CPU time scales linearly with then

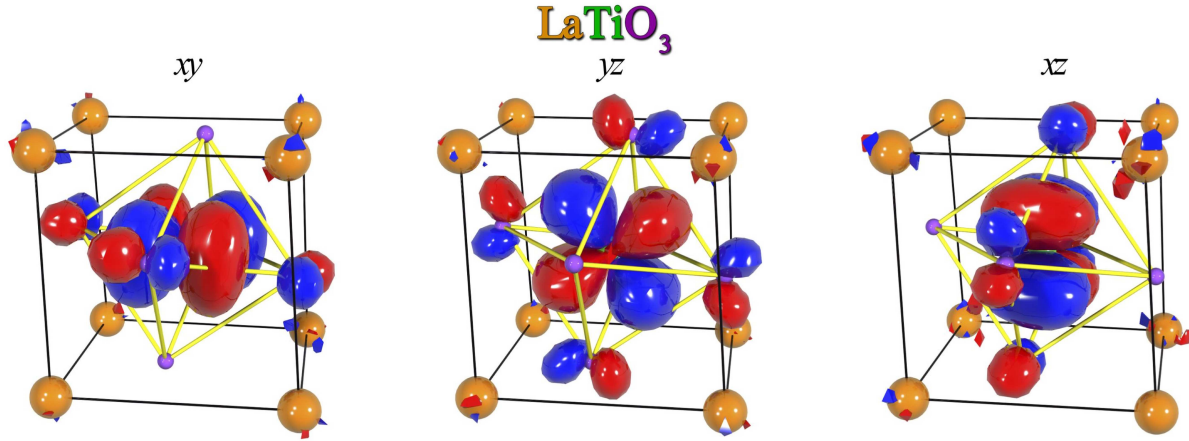


**Fig. 5:** Contour plot of the  $t_{2g}$  Wannier functions for  $\text{LaTiO}_3$ . The spheres represent the atoms: La (orange), Ti (green), O (blue). From Ref. [20].

number of sweeps and scales with the third power of the number of slices. As a rule of thumb,  $U\beta/L \sim 1/2$  usually yields a reasonably small Trotter error; thus, the lower the temperature the large should be  $L$ . Therefore QMC simulations are often performed at high temperatures ( $T \sim 500\text{-}1000$  K); these temperatures are usually appropriate for studying the paramagnetic phases of strongly correlated metals and Mott insulator. Supercomputers make lower temperatures accessible. For the  $T = 0$  case other impurity solvers (e.g. exact diagonalization) are used.

## 4.2 LDA+DMFT

Recently it has been suggested that DMFT could be used in combination with LDA [15] to study realistic model Hamiltonians. The basic idea is to use the LDA density of states (DOS), projected onto the correlated orbitals, as a input for DMFT calculations, and then proceed as described in the previous session. LDA+DMFT was applied with success to many materials. This implementation of LDA+DMFT is however useful for one-band cases and/or for cubic multiband systems only. However, many interesting strongly correlated systems have many bands and lower symmetry. The implementation of a general LDA+DMFT scheme requires (i) a method for constructing material-specific multiband Hubbard Hamiltonians and (ii) an appropriate DMFT impurity solver for such a multi-band Hubbard model. Recently such a LDA+DMFT scheme has been implemented using (i) NMTO Hamiltonians and (ii) a generalized Hirsch-Fye quantum Monte Carlo algorithm[19].

The local Green function matrix is obtained as

$$G(\tau) = \sum_n \exp(-i\omega_n\tau) \sum_{\mathbf{k}} \frac{1}{i\omega_n + \mu - H_{\mathbf{k}}^{\text{LDA}} - \Sigma(i\omega_n)} \quad (45)$$

where  $H_{\mathbf{k}}^{\text{LDA}}$  is the LDA Hamiltonian for the correlated electrons (obtained downfolding all the states but the correlated orbitals). Here the self energy, the bath Green function and the impurity Green function are all *matrices*.

The procedure is similar to the one described in the previous session; the bath Green function matrix,  $\mathcal{G}_0$ , is obtained from Eq. (37), and from  $\mathcal{G}_0$  the quantum impurity model is defined



through the effective action  $S_{\text{eff}}$ . For a  $M$ -band Hubbard model, however, in order to decouple the on site Coulomb interaction for each time slice,  $M(2M - 1)$  Ising fields are required. Clearly, this means that the CPU time can increase dramatically when the number of orbitals increase. The  $G$  matrix obtained from QMC is then used to calculate the new self-energy, and therefore the new bath Green function matrix, till self-consistency on the self-energy is reached. The LDA+DMFT approach described above is very general and can be successfully used to study transition metal oxides and  $f$  electron systems. Before we discuss a recent application of this method, it is important to underline two points.

The Hubbard model Eq. (5) is the sum of a kinetic energy and a correlation term; in LDA+DMFT the kinetic energy is obtained from LDA, thus *some* of the electron-electron correlations explicitly described by the Coulomb interaction are also included in the kinetic energy term. To avoid double-counting, a correction should be added to subtract the LDA contribution; unfortunately, this correction is unknown. There is a case in which the double-counting correction is just a shift of the chemical potential: the case in which the LDA Hamiltonian describes e.g. *only* strongly correlated  $d$  electrons and the weakly correlated states are all downfolded. Therefore, this is the most common approach to LDA+DMFT. In many cases, however, it is necessary to work in a larger basis, which includes both correlated and uncorrelated channels. If this is the case (see e.g. a recent implementation of LDA+DMFT [16]), the double counting correction has to be explicitly included; different recipes to calculate this correction are commonly used. Finally, it is worth to underline that, within the Hirsh-Fye QMC scheme, the exchange Coulomb interaction in Eq. (5) is usually approximate to the density-density term only

$$\hat{U} = U \sum_{im} n_{im\uparrow} n_{im\downarrow} + (U - 2J) \sum_{i(m \neq m')} n_{im\uparrow} n_{im'\downarrow} + (U - 3J) \sum_{i\sigma(m \neq m')} n_{im\sigma} n_{im'\sigma}. \quad (46)$$

The spin-flip terms in the exchange interaction are neglected. This approximation is adopted because the (small) spin-flip terms can give rise to a sign problem; new QMC algorithms which can treat the full exchange interaction (e.g. continuous-time quantum Monte Carlo) are however under development. In Eq. 46 we also adopted the common assumption that, as in the isotropic case,  $U_{mm} = U$ ,  $U_{mm'} = U - 2J$  and  $J_{mm'} = J$ .

## 5 Application to orthorhombic $3d^1$ perovskites

The series of strongly correlated  $3d^1$  perovskites, which includes  $\text{SrVO}_3$ ,  $\text{CaVO}_3$ ,  $\text{LaTiO}_3$  and  $\text{YTiO}_3$ , has been studied for decades for their unusual electronic and magnetic properties, arising from narrow  $3d$  bands and strong electron-electron interaction. These systems are particularly interesting because they are very similar and still display very different properties.

We have already described  $\text{SrVO}_3$ ; this material is a cubic perovskite and its primitive cell includes a single  $\text{VO}_6$  octahedron, at the center of a  $\text{Sr}$  cubic cage. The other systems ( $\text{CaVO}_3$ ,  $\text{LaTiO}_3$  and  $\text{YTiO}_3$ ) exhibit the  $\text{GdFeO}_3$  distortion: the octahedra tilt around a  $[100]$  axis and rotate around a  $[001]$  axes, the cation cage is distorted and the primitive cell includes 4 octahedra. Going along the series ( $\text{SrVO}_3 \rightarrow \text{CaVO}_3 \rightarrow \text{LaTiO}_3 \rightarrow \text{YTiO}_3$ ) the  $\text{GdFeO}_3$  distortion increases; furthermore, the strength of correlation effects (measured by the mass renormalization in metals and by the Mott gap in insulators) increases too, and a metal-insulator transition occurs between  $\text{CaVO}_3$  and  $\text{LaTiO}_3$  [6].

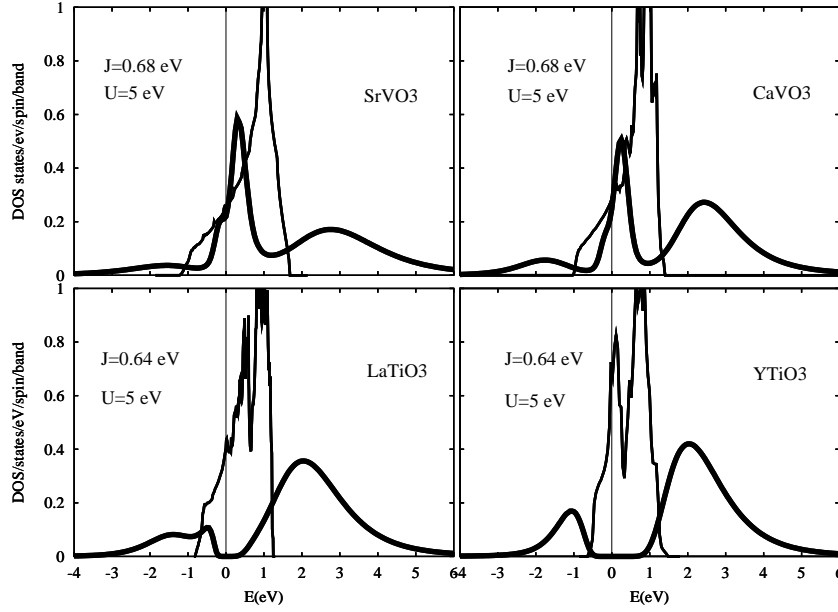


**Fig. 6:** The LDA+DMFT spectral function at 770 K (thick line) vs. the LDA density of states (thin line). From Ref. [19]

In order to understand this Mott metal-insulator transition we used the LDA+DMFT technique described in the previous session [19, 20]. Here I will summarize only some of the results.

First we obtained the LDA electronic structure with the NMTO method. In all the  $3d^1$  perovskites the  $t_{2g}$  LDA bands are occupied by one electron and well divided from the empty  $e_g$  bands and the filled O bands, as shown in Fig. 2 for  $\text{SrVO}_3$ . Thus we downfolded all the degrees of freedom but the  $t_{2g}$  and we obtained the LDA Hamiltonian and the NMTO Wannier functions for the  $t_{2g}$  bands. The  $t_{2g}$  NMTOs are displayed in Fig. 5 for  $\text{LaTiO}_3$ . We found that the  $t_{2g}$  band width,  $W$ , decreases going from  $\text{SrVO}_3$  to  $\text{YTiO}_3$  [20]. This is visible in Fig. 6 where the LDA DOS is shown for each system. We calculated the spectral function by means of LDA+DMFT for several values of  $U$  between 3 eV and 6 eV. The Mott transition was reproduced rather well for  $U \sim 5$  eV, the same for all materials (see Fig. 6); this is satisfying, because  $U$  is expected to be similar in vanadates and titanates [17]. For this value of  $U$ ,  $\text{SrVO}_3$  and  $\text{CaVO}_3$  are metallic with a mass renormalization 2.2 and 3.5 respectively, in reasonable agreement with the values obtained from optical conductivity (2.7 and 3.6); the titanates are insulators,  $\text{LaTiO}_3$  with a small (0.3 eV) gap and  $\text{YTiO}_3$  with a larger gap (1 eV), again in agreement with experiments. The position of the LHB is around -1.8 eV for  $\text{SrVO}_3$  and  $\text{CaVO}_3$  and around -1.5 eV for the insulators, in very good agreement with photoemission data [6]. The analysis of the spectral function matrix (Fig. 7) provides further insight. We found that, in the insulators, only one orbital is occupied, the lowest energy crystal field orbital (different for  $\text{YTiO}_3$  and  $\text{LaTiO}_3$ ). In LDA, this orbital is *only*  $\sim 120$  meV ( $\text{LaTiO}_3$ ) and  $\sim 200$  meV ( $\text{YTiO}_3$ ) lower in energy than the other two; thus orbital fluctuations are large. Electron-electron repulsion strongly suppresses these fluctuations, as Fig. 7 shows: only the lowest energy (red) level is occupied. The effect of the small crystal field splitting is surprisingly strong, but it can be understood by analyzing the influence of orbital degrees of freedom on the Mott transition. It is known that the critical ratio  $(U/W)_c$  increase with orbital degeneracy [21]. Close to the Mott transition, the quasiparticle peak has a width  $\sim ZW$ , with  $Z \sim 1 - U/U_c$ . Thus, although rather small compared to  $W$  and

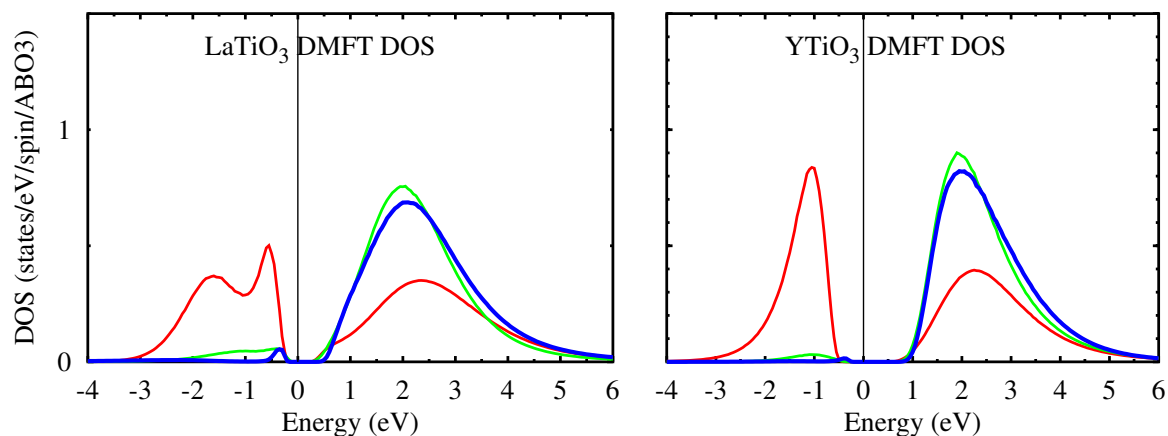


**Fig. 7:** The orbital resolved spectral function of  $\text{LaTiO}_3$  and  $\text{YTiO}_3$  for  $U = 5 \text{ eV}$  and in the basis which diagonalized the DMFT occupation number matrix. These states turned out to be similar to the crystal field levels, with the most occupied state (red curve) corresponding to the lowest LDA energy level. From Ref. [20]

$U$ , a crystal field splitting of the order of  $\sim ZW$  reduces the orbital degeneracy (in the extreme case, from a three to a one band model), and favors the transition to a Mott insulating orbitally ordered state [22].

## 6 Concluding remarks

In this lecture I have briefly presented the modern approach to the theory of strongly correlated systems, the so-called LDA+DMFT method. In this approach optimal many-body model Hamiltonian are constructed from first principles, and then solved by means of the dynamical mean field theory (DMFT). I have shown that Nth-order Muffin Tin Orbital (NMO) Wannier functions are a suitable basis for building small but realistic models. Other types of Wannier functions [12, 16] are currently available and/or under development.

Although rather successful in describing the low-temperature physics of many correlated oxides, LDA+DMFT is only a first step towards a theory with predictive power for strongly correlated materials. Many questions are still open. An important issue is establishing a reliable scheme to calculate the screened Coulomb interaction [18]. A related problem is finding the best set of Wannier function, those that minimize the range of the electron-electron repulsion. Furthermore, spatial fluctuations are important for many correlated materials and many phenomena: spin waves in magnetic systems, phase transitions with non local order parameters, the competition between magnetism and Kondo effect in heavy fermions. These effects cannot be described by a local self-energy. To correct this flaw different types of *cluster* extensions of dynamical mean field theory (CDMFT) have been suggested and are already used. Finally, there are proposals of going beyond model Hamiltonians, getting rid of parameters, e.g. the GW+DMFT [23] scheme. There is still a lot to do before a fully *ab-initio* theory for strongly correlated systems will be available.

## Appendices

### A Atomic units

The atomic units can be obtained as follows. In the MKS units system  $\hbar = h/4\pi$ , the electron mass  $m_e$ , the electron charge  $e$ ,  $4\pi\epsilon_0$  have the following values

$$\begin{aligned}\hbar &\sim 1.0546 \cdot 10^{-34} \text{ Js} & [ML^2T^{-1}] \\ m_e &\sim 9.1094 \cdot 10^{-31} \text{ kg} & [M] \\ e &\sim 1.6022 \cdot 10^{-19} \text{ C} & [Q] \\ 4\pi\epsilon_0 &\sim 1.1127 \cdot 10^{-10} \text{ F/m} & [M^{-1}L^{-3}T^2Q^2], .\end{aligned}$$

The dimensions of each constant are written on the right. We now want to define a system of units in which the four constants above are all 1,  $\hbar = m_e = e = 4\pi\epsilon_0 = 1$ . Thus we have to solve the following system of equations

$$\begin{aligned}\hbar &= 1 \cdot a_0^2 m_e / t_0 \\ m_e &= 1 \cdot m_0 \\ e &= 1 \cdot e_0 \\ 4\pi\epsilon_0 &= 1 \cdot t_0^2 e^2 / a_0 m_e^3\end{aligned}$$

where  $a_0$  is 1 atomic unit of length,  $t_0$  1 atomic unit of time, and so on. The solution of this system yields

$$\begin{aligned}1 \text{ a.u. length} &= a_0 = \frac{4\pi\epsilon_0}{m_e e^2} \sim 5.2918 \cdot 10^{-11} \text{ m} \\ 1 \text{ a.u. mass} &= m_0 = m_e \sim 9.1094 \cdot 10^{-31} \text{ kg} \\ 1 \text{ a.u. charge} &= e_0 = e \sim 1.6022 \cdot 10^{-19} \text{ C} \\ 1 \text{ a.u. time} &= t_0 = \frac{(4\pi\epsilon_0)^2 \hbar^3}{m_e e^4} \sim 2.4189 \cdot 10^{-17} \text{ s}.\end{aligned}$$

## References

- [1] See Science special issue *Correlated Electron Systems*, Science **288**, (2000).
- [2] P. Hohenberg and W. Kohn, Phys. Rev. **136**, B864-B871 (1964).
- [3] W. Kohn and L.J. Sham, Phys. Rev. **140**, A1133-A1138 (1965).
- [4] O. Gunnarsson and B. I. Lundqvist, Phys. Rev. B **23**, 4274 (1976).
- [5] W. Kohn, Rev. Mod. Phys. **71**, 1253 (1999).
- [6] M. Imada, A. Fujimori, and Y. Tokura, Rev. Mod. Phys. **70**, 1039 (1998).
- [7] W. Metzner and D. Vollhardt, Phys. Rev. Lett. **62**, 324 (1989).
- [8] A. Georges, G. Kotliar, W. Kraut, M.J. Rozenberg, Rev. Mod. Phys. **68**, 13 (1996).
- [9] J.E. Hirsch and R.M. Fye, Phys. Rev. Lett. **56**, 2521 (1986).
- [10] O.K. Andersen and T. Saha-Dasgupta, Phys. Rev. B **62**, R16219 (2000); O.K. Andersen, T. Saha-Dasgupta, R.W. Tank, C. Arcangeli, O. Jepsen, G. Krier, in: *Electronic Structure and Physical Properties of Solids: The uses of the LMTO method*, Ed. H. Dreyssé, Springer, Lecture Notes in Physics **535**, 3-84 (2000).
- [11] W. Kohn and J. Rostoker Phys. Rev. **94**, 1111 (1954).
- [12] N. Marzari and D. Vanderbilt, Phys. Rev. B **56**, 12847 (1997).
- [13] Here, for simplicity, we discuss the solution of the Schrödinger equation. Most *ab-initio* study, however, require the solution of the Dirac equation, or exact (fully relativistic scheme) or approximate (e.g. the scalar relativistic approximation is often used).
- [14] J.E. Gubernatis, M. Jarrel, R.N. Silver and D.S. Sivia Phys. Rev. B **44**, 6011 (1991).
- [15] V. Anisimov, A. Poteryaev, M. Korotin, A. Anokhin, and G. Kotliar, J.Phys: Condens. Matter **9**, 7359 (1997); A.I. Lichtenstein and M.I. Katsnelson, Phys. Rev. B **57** 6884 (1998).
- [16] V. Anisimov *et al.*, Phys. Rev. B **71**, 125119 (2005).
- [17] T. Mizokawa and A. Fujimori, Phys. Rev. B **54** 5368 (1996).
- [18] F. Aryasetiawan, M. Imada, A. Georges, G. Kotliar, S. Biermann, A. I. Lichtenstein, Phys. Rev. B **70**, 195104 (2005); M. Cococcioni, S. de Gironcoli, Phys. Rev. B **71**, 035105 (2005) .
- [19] E. Pavarini, S. Biermann, A. Poteryaev, A.I. Lichtenstein, A. Georges, O.K. Andersen, Phys. Rev. Lett. **92**, 176403 (2004).
- [20] E. Pavarini, A. Yamasaki, J. Nüss and O. K. Andersen, New J. Phys. **7**, 188 (2005).

- [21] O. Gunnarsson, E. Koch and R.M. Martin, Phys. Rev. **54**, 11026 (1996); O. Gunnarsson, E. Koch and R.M. Martin, Phys. Rev. B **56** 1146 (1997); S. Florens, A. Georges, G. Kotliar and O. Parcollet, Phys. Rev. B **66**, 205102 (2002).
- [22] N. Manini, G.A. Santoro, A. Dal Corso and E. Tosatti, Phys. Rev. B 115107 **66** (2002).
- [23] S. Biermann, F. Aryasetiawan, A. Georges, Phys. Rev. Lett. **90**, 086402 (2003).